Using Nanocomposite Coatings To Heal Surface Defects

Sandeep Tyagi, Jae Youn Lee, Gavin A. Buxton, and Anna C. Balazs*

Department of Chemical and Petroleum Engineering, University of Pittsburgh, Pittsburgh, Pennsylvania 15261

Received June 21, 2004; Revised Manuscript Received September 24, 2004

ABSTRACT: Using computer simulations, we investigate the benefits of coating substrates that contain nanoscale defects with nanoparticle-filled polymer films. In particular, we focus on surfaces that contain a nanoscopic notch and use molecular dynamics (MD) simulations to determine the particle and polymer distribution on the damaged surface. The calculations reveal that a high volume fraction of relatively large particles are localized in the notch. Here, the polymer melt induces a depletion attraction between the particles and surface and thereby drives the nanoparticles into the defect. The time required for these relatively large particles to migrate to the notch is comparable to the time needed for the chains to move by approximately four radius of gyrations. The morphology obtained from the MD simulation serves as the input to the lattice spring model (LSM), which allows us to determine the mechanical properties of the nanocomposite-coated surface. The results show that the stress concentration at the notch tip is significantly reduced due to the presence of the nanoparticles. The application of such nanocomposite coatings could potentially yield defect-free surfaces that exhibit enhanced mechanical properties.

I. Introduction

During the manufacturing of various components, nanoscale defects and scratches can appear on the surface of the material. Because of the small size scale of these defects, they are difficult to detect[1] and consequently difficult to repair. However, such defects can have a substantial effect on the mechanical properties of the system. For example, significant stress concentrations can occur at the tip of notches in the surface; such regions of high stress can ultimately lead to the propagation of cracks through the system and the degradation of mechanical behavior.

A possible means of repairing these nanoscale defects is to coat the surface of the manufactured component with a polymer melt that contains nanoparticles. The particles can potentially migrate to and fill the nanoscopic scratches and notches. The system can then be cooled so that the coating forms a solid nanocomposite layer that effectively repairs the flaws in the surface.

To test this concept, we use molecular dynamics (MD) simulations to model the structural evolution and final morphology of the system illustrated in Figure 1. A mixture of polymeric chains and particles is confined between two hard walls. The top wall serves to constrain the polymers and particles into a thin film. The bottom wall represents the damaged surface; it contains a well-defined notch that penetrates into the underlaying solid material. Initially, the particles are randomly dispersed in the polymer matrix. In previous studies of confined films of nanoparticle-filled polymers,[2,3] we found that the polymers induce an entropic "depletion attraction"[4−6] between the particles and the confining surfaces. In particular, the polymers in the thin films expel a fraction of the particles to the walls; in this way, the chains gain conformational entropy because they do not have to stretch around particles within the film.[2,3,7]

To our knowledge, there have been few studies of such "depletion forces" in particle-filled polymer films.[2,3,8] We note, however, that similar entropic effects are seen when binary particle mixtures are dispersed in a diblock copolymer melt.[9−11] While the large and small nanoparticles in the particle mixture are chemically compatible with the A block of the AB diblocks, both theoretical[9,10] and experimental studies[11] show that the larger particles are expelled to the interface *between* the A brushes. By driving the larger particles to this interface, the A blocks need not extend around these fillers, and the polymers' loss in conformational entropy is mini-

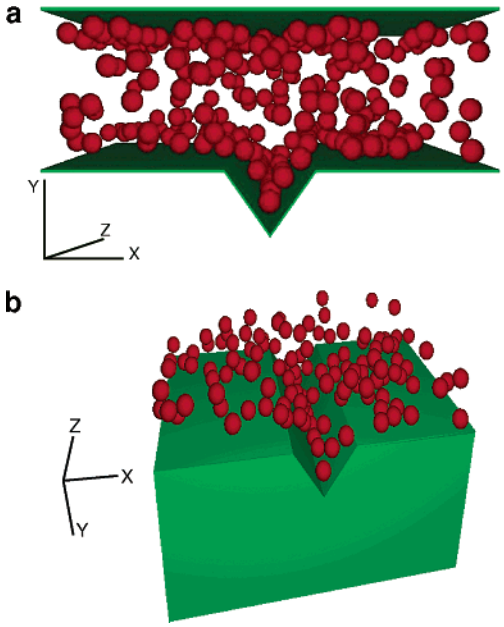

Figure 1. Geometry of the system used in the molecular dynamics (MD) simulations. The particles are displayed as red spheres, and the confining walls are shown in green; for clarity, the polymers are not depicted. Here, the diameter of the particles is $\sigma_p = 1.7\sigma$. The images are for a fully equilibrated system. The figure in (a) shows the full simulation box. The figure in (b) is viewed from a different angle and shows the portion of the MD simulation that is fed into the lattice spring model (LSM). Note that (b) reveals a string of particles that are localized in the tip of the notch.

* To whom correspondence should be addressed. E-mail: balazs1@engr.pitt.edu.

10.1021/ma048773l CCC: $27.50
Published on Web 11/06/2004

mized.[9,10,12] In effect, the A blocks act as depletants, which give rise to a depletion attraction between the larger particles and promote the flocculation of these particles at the interface.[12] The smaller particles do not perturb the conformation of the chains, and thus, they remain localized *within* the A brushes.

Related to this issue is the common challenge in fabricating filled polymer systems: it is difficult to disperse the filler particles within polymer melts, even when the polymers and particles are chemically compatible.[13,14] Within these systems, the polymers drive the aggregation of the particles and thereby enhance the volume that is accessible to the chains. In other words, the aggregation of the fillers is also driven by an entropically induced depletion attraction that is caused by the polymers in the melt.

In contrast to the situation in polymer melts, there have been extensive, fundamental studies of depletion attraction between colloids and confining surfaces in polymeric solutions or simple solvents.[15,16] Studies that are particularly relevant to our investigation involved a solution containing a binary colloid mixture lying above a regular, rough surface.[17−19] To gain translational entropy, the smaller spherical colloids essentially "pushed" the larger spheres into the depressions or wells in the rough surface. (In one of these studies,[17] a nonadsorbing polymer chain constituted the smaller colloid.) These findings indicate that particles in solution can be manipulated to localize in specific regions of a surface.

Using the MD simulations, we examine the extent to which the confined polymer melt in Figure 1 can induce a depletion attraction between the particles and surfaces and thereby drive the particles into the nanoscale notch in the lower wall. We then isolate the conditions that enhance the concentration of particle fillers within the damaged region.

Once we obtain the equilibrium structure of the mixture from the MD simulations, we then use this information as the input into a micromechanics simulation in order to evaluate how the fillers modify the mechanical behavior of the system. Here, we assume that the filled melt is rapidly cooled to form the solid coating and that the morphology does not change under the rapid quench. Consequently, the location of the particles and polymers in the MD lattice is mapped onto the lattice spring model (LSM), which consists of a three-dimensional network of harmonic springs. We assign a different spring constant, k, to springs localized in polymer domains and to springs located in particle regions. We then apply a stress at the boundaries of the simulation box and determine the local elastic response of the system. In this manner, we can correlate the particle distribution within the film to the mechanical properties of the material. Furthermore, by comparing the properties of particle-filled and unfilled polymer coatings, we can isolate the effect of the fillers on the mechanical behavior and determine the extent to which the particles effectively repair the damaged substrate.

Below, we begin by describing the details of the MD and LSM simulations. We then discuss the effect of varying particle size on the localization of the particles into the notch. Next, we compare the mechanical properties of the particle-filled and unfilled systems. These findings provide guidelines for formulating nanocomposite coatings that effectively heal the surfaces through the self-assembly of the particles into the defects. Ideally, this coating could be applied as a final processing step, with subsequent cooling to harden the film and produce this healing layer.

II. The Models

A. Molecular Dynamics Simulation. As noted in the Introduction, we use MD simulations to obtain the dynamic behavior and equilibrium structure of a thin film of polymers and nanoparticles. In our model, the polymers are modeled as bead−spring chains. Each chain is composed of 40 Lennard-Jones (LJ) spheres, of mass m and diameter σ, that are connected by anharmonic springs. The nanoparticles are treated as LJ spheres of mass m_p and diameter σ_p.

Each sphere i interacts with another sphere j (of the same or different type) through a truncated LJ potential of the form

$$U_{LJ}(r) = \begin{cases} 4\epsilon_{ij}\left[\left(\frac{\sigma_m}{r}\right)^{12} - \left(\frac{\sigma_m}{r}\right)^{6} - \left(\frac{\sigma_m}{r_c}\right)^{12} + \left(\frac{\sigma_m}{r_c}\right)^{6}\right] & r \le r_c \\ 0 & r > r_c \end{cases} \quad (2.1)$$

where $\sigma_m = (\sigma_i + \sigma_j)/2$. Here, ϵ_{ij} is the characteristic interaction energy between spheres i and j. The potential is cut off at its minimum $r_c = 2^{1/6}\sigma_m$ to yield a purely repulsive interaction. The cutoff distance is chosen to save computational time (not to indicate chemical incompatibility);[20] this choice has been shown to recover the correct liquid behavior in dense polymeric melts.[21] In addition, by setting all $\epsilon_{ij} = \epsilon = 1$ in this form of the potential, we can focus on systems where entropy, and consequently the depletion forces, will play a significant role.

Adjoining spheres along a chain, separated by a distance r, interact through a finite extendable nonlinear elastic (FENE) potential of the form

$$U_{FENE}(r) = \begin{cases} -0.5\kappa {R_0}^2 \ln\left[1 - \left(\frac{r}{R_0}\right)^2\right] & r < R_0 \\ \infty & r \ge R_0 \end{cases} \quad (2.2)$$

where $\kappa = 30\epsilon/\sigma^2$ is the spring constant and $R_0 = 1.5\sigma$. These values ensure that the chains do not break or cross at the temperature considered in this study.

As depicted in Figure 1, the polymer/particle mixture is confined in the y direction by two walls. The lower wall contains a notch, which represents a nanoscale defect. The maximum width at the top of the notch (along the x axis) is 6σ, and the depth (along the y axis) is 4σ. The dimensions of the simulation box are $30\sigma \times 10\sigma \times 20\sigma$ (excluding the notch), and periodic boundary conditions are applied in the directions normal to the confinement. The confining walls are modeled as smooth, continuous surfaces that interact with the polymer beads and nanoparticles through a purely repulsive potential, whose form is given in the Appendix.

The simulations are performed at a constant temperature of $T^* = kT/\epsilon$, which is maintained by a Brownian thermostat. The equation of motion for the displacement of a monomer or filler i is given by

$$m_i \frac{d^2\mathbf{r}_i}{dt^2} = -\nabla_i U - m_i \Gamma \frac{d\mathbf{r}_i}{dt} + \mathbf{W}_i(t) \quad (2.3)$$

where U is the total potential energy felt by sphere i

(for a polymer bead $U = U_{LJ} + U_{FENE} + U_{wall}$, and for a particle $U = U_{LJ} + U_{wall}$). The parameter $\mathbf{W}_i(t)$ is a stochastic force that is related to the friction coefficient by the fluctuation−dissipation theorem and is described by ref 21:

$$\langle W_{i\alpha}(t)\, W_{j\beta}(t')\rangle = \delta_{ij}\delta_{\alpha\beta}\delta(t-t')2k_BT\Gamma \qquad (2.4)$$

Here, the friction coefficient Γ for monomers is $\Gamma = 0.5\tau^{-1}$, where $\tau = \sigma\sqrt{m/\epsilon}$ is the characteristic LJ time. Similarly, for filler particles, $\Gamma_p = 0.5\tau_p^{-1}$, with $\tau_p = \sigma_p\sqrt{m_p/\epsilon}$. The above equation of motion is solved by the velocity Verlet algorithm with a time step of 0.010τ. It is normal practice in MD simulations[20,21] to use time steps in the range of 0.006τ to 0.012τ. We also carried out simulations with a time step of 0.006τ. We found no difference between the final results that were obtained with the different time step values.

The parameters ρ and ρ_p denote the density of monomers and particles, respectively. To model a relatively dense system, we fix the overall reduced density of the composite at 0.83, where the reduced density of the monomers is $\rho\sigma^3 = 0.66$ and that of the nanoparticles is $\rho_p\sigma_p^3 = 0.17$. It should be noted that the volume fraction of a species is obtained by multiplying the reduced density by a factor of $\pi/6$.

The starting configuration of the polymers is obtained from a random walk of chains constrained between the walls, where the bond lengths and angles are chosen appropriately.[21] The nanoparticles are added to the system at random positions, resulting in a configuration where monomers and nanoparticles overlap. This overlapping is removed by replacing the LJ potential with a softer cosine potential

$$U_{soft}(r) = \begin{cases} A\left[1 + \cos\left(\dfrac{\pi r}{r_c}\right)\right] & r \le r_c \\ 0 & r > r_c \end{cases} \qquad (2.5)$$

where A is a repulsion factor, which is gradually increased from 1 to 60. This increase in the value of A amounts to slowly increasing the repulsion from zero to a value that ensures that no beads overlap.

The system is allowed to evolve for 1−2 million MD time steps (depending on particle size) before taking any measurements, ensuring that the system is well equilibrated. During this time, the center of mass (CM) for chains is displaced by a distance that is at least 5 times the radius of gyration of the chains. The measurements are accumulated over the next 2 million MD time steps.

B. Lattice Spring Model. Once we obtain the equilibrium structure of the system, we use this information as the input into the lattice spring model (LSM).[22−26] We utilize a Born LSM[27] in order to capture the micromechanical deformation of the coated substrate in a computationally efficient manner. The LSM is a numerical technique for discretizing linear elasticity theory and consists of a network of springs connecting regularly spaced sites, or nodes. The energy associated with the mth node is given by ref 27

$$E_m = \frac{1}{2}\sum_n (\mathbf{u}_m - \mathbf{u}_n)\cdot\mathbf{M}_{mn}\cdot(\mathbf{u}_m - \mathbf{u}_n) \qquad (2.6)$$

where the summation is over all nearest- and next-nearest-neighboring nodes. Here, $\mathbf{u}_m$ is the displacement of the mth node from its original position, and $\mathbf{M}_{mn}$ is a matrix containing the force constants (stiffness) for the spring between nodes m and n. The springs have two different types of force constants, central and noncentral. The central force constant energetically penalizes spring extension, while the noncentral force constant penalizes the rotation of springs from their original orientation. The Young's modulus, E, and Poisson's ratio, ν, are related to the force constants by the following equations:[27]

$$E = \frac{5k(2k+3c)}{4k+c} \qquad \nu = -\frac{k-c}{c+4k} \qquad (2.7)$$

where k and c are the central and noncentral force constants, respectively. The force constants are initially associated with the nodes. Nodes are assigned different values depending upon their location in the material. In particular, $k = 100$ in the substrate and particles and $k = 1$ in the polymer matrix. This choice for the relative stiffness of the different components is consistent with experimental values for particles and polymers in filled polymeric systems.[13] The force constants assigned to the springs are then averaged from the nodes that they connect. Here, we set $c = 0$, yielding a value of $\nu = -1/4$ in both the polymer and particulate regions. This choice can be justified by noting that stress and strain concentrations in heterogeneous materials generally occur due to local variations in Young's modulus, while local variations in Poisson's ratio induce negligible perturbations to the elastic fields.

The harmonic form of the energy in eq 2.6 results in a force term that is linearly related to the displacements. The force acting on the mth node, due to the local displacements of its neighboring nodes, is given by

$$\mathbf{F}_m = \sum_n M_{mn}\cdot(\mathbf{u}_m - \mathbf{u}_n) \qquad (2.8)$$

If forces are applied to the boundary nodes, and the spring constants specified, then the nodal displacements can be obtained through a set of sparse linear equations. These equations are solved using a conjugate gradient method to find the equilibrium configuration that corresponds to no net force at each node.[22−28]

To present relevant deformation fields, the stress and strain tensors are calculated from the forces and displacements. The strain tensor can be obtained through a finite difference approximation of the displacement field. A central difference approximation can be used to obtain this strain tensor:[27]

$$\delta_x u_{(i,j,k)} = \frac{-u_{(i+2,j,k)} + 8u_{(i+1,j,k)} - 8u_{(i-1,j,k)} + u_{(i-2,j,k)}}{12d} \qquad (2.9)$$

where $u_{(i,j,k)}$ is the displacement field at coordinates i, j, k, and d is the initial distance between adjacent nodes; alternatively, forward or backward approximations are considered at system boundaries. The stress tensor is directly obtainable from the forces acting on a node (the center of a cubic unit cell)[29]

$$\sigma_{ij} = \frac{\sum_m F_m n_{ij}^{\ m}}{A} \qquad (2.10)$$

Here, Σ_m represents a sum over the cubic surfaces and

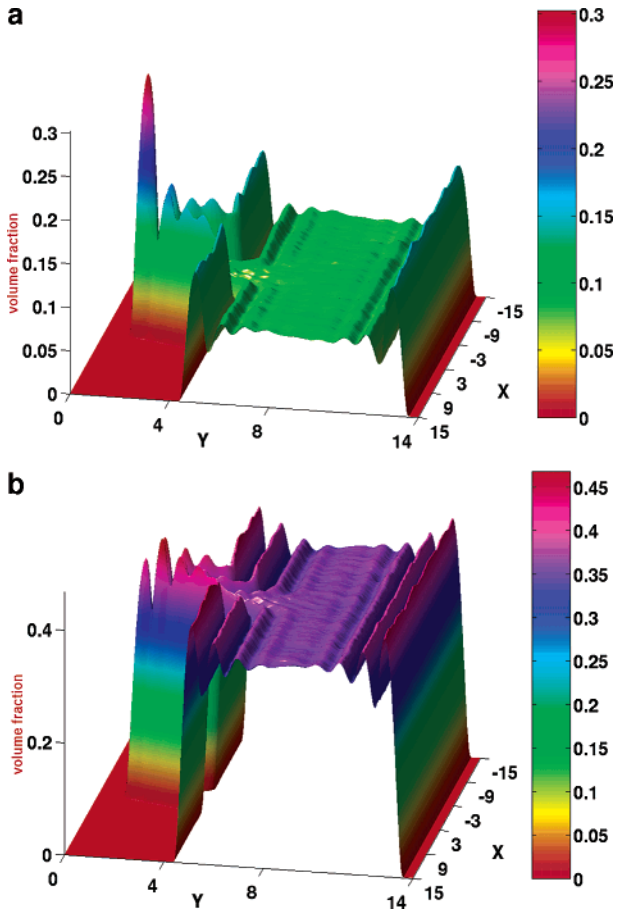

Figure 2. Two-dimensional profiles depicting the average volume fractions of the following: (a) particles of size $\sigma_p = \sigma$ and (b) polymers. The data are averaged over 20 000 configurations and the range of z values.

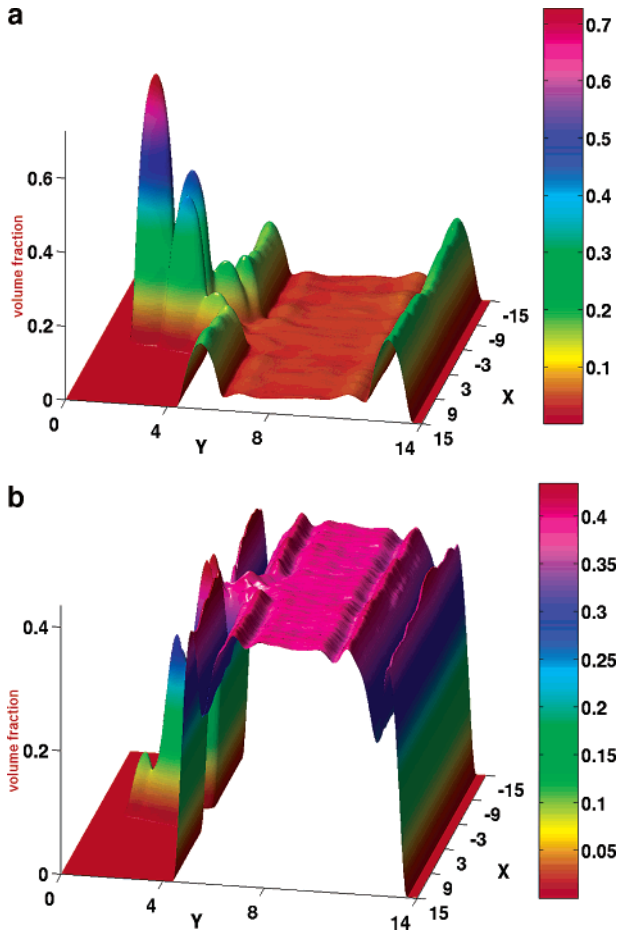

Figure 3. Two-dimensional profiles depicting the average volume fraction of the following: (a) particles of size $\sigma_p = 1.7\sigma$ and (b) polymers. The data are averaged over 20 000 configurations and the range of z values.

F_m is the force on any surface m of the cubic cell, while n_{ij}^m is a unit vector either normal or parallel to the surface m and A is the surface area. The scalar stress and strain values quoted here correspond to the normal stress and strain components in the tensile direction.

III. Results and Discussion

A. Morphology of Film. We consider a range of particle sizes (from $\sigma_p = \sigma$ to $\sigma_p = 1.8\sigma$), while keeping the size of the monomers fixed. Below, we focus our discussion on the results from two different particle sizes, $\sigma_p = \sigma$ and $\sigma_p = 1.7\sigma$.

For the smallest particle size considered in this study, where the nanoparticles are the same size as the monomers, the system consists of 3760 monomers and 940 filler particles. Figure 2 shows the volume fractions of these small particles and the polymers for the equilibrated system. Figure 2a reveals that the particles are relatively localized at the walls and within the tip of the notch. Within these areas of higher particle concentration, the volume fraction is roughly 1.5−3 times higher than the uniform distribution (with the uniform volume fraction corresponding to the input value of $0.17 \times \pi/6 = 0.09$). Figure 2b shows that the polymers are more uniformly distributed throughout the sample than the nanoparticles. However, while the particles are primarily located at the tip, the polymers fill the entire notch. Another noticeable feature is the short-range ordering of polymers at the surfaces, resulting in a rippling effect in the polymer volume fraction profile. (Similar effects are seen to a lesser extent among the particles in Figure 2a.)

For the larger particle size, $\sigma_p = 1.7\sigma$, there is a total of 3760 monomers and 191 particles in the system. The particle volume fraction is shown in Figure 3a, and the polymer volume fraction is shown in Figure 3b. If we compare the volume fraction distributions for the larger and smaller particles, we see distinct differences. In the case of the larger particles, there is a sharp increase in the particle concentration at the tip of the notch as well as a smaller increase along the flat walls. In these studies, the polymer/nanoparticle mixture constitutes a dense system. Thus, if the particle concentration at the notch is significantly increased, the polymer volume fraction is decreased. This fact accounts for the dips in the polymer concentration at the solid walls in Figure 3b.

To further appreciate the effect of the particle size on the localization of these fillers at the defect site, we plot the relative volume fraction of particles inside the entire volume of the notch (not just the notch tip) as a function of σ_p in Figure 4. We consider two different notch sizes, the one used in Figures 1−3 and a larger notch, where the depth is 6.8σ and the width is 10.2σ. (The latter numbers were chosen so that the notch size is scaled by the size of the larger particle, $\sigma_p = 1.7\sigma$.) For the case where the particle size is the same as the monomer size, the volume fraction inside the notch is nearly the same as outside and matches the overall volume fraction. However, the volume fraction of the

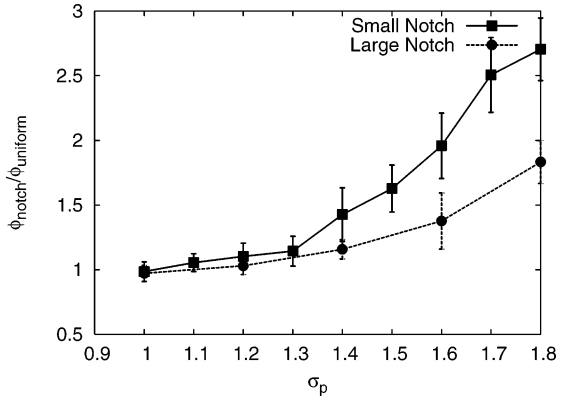

Figure 4. Average volume fraction of particles inside the notch ($\phi_{notch}/\phi_{uniform}$) as a function of particle size for two different notch sizes. For uniformly distributed particles, the volume fraction would equal 0.09.

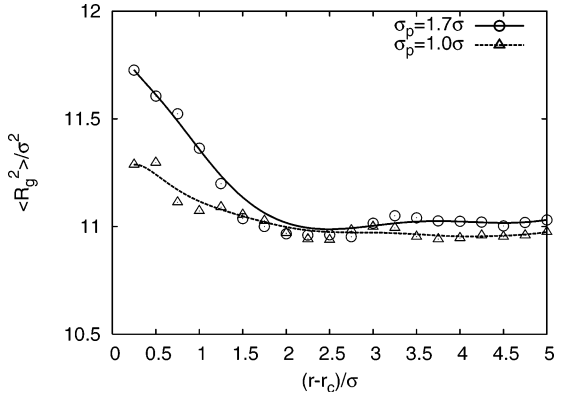

Figure 5. Average of the square of the radius of gyration, $\langle R_g^2 \rangle$, as a function of the distance from the particle surface to the center of mass of a chain. To make the value dimensionless, we divide $\langle R_g^2 \rangle$ by σ^2. The data are plotted for two particle sizes, $\sigma_p = \sigma$ and $\sigma_p = 1.7\sigma$. The lines, which are a fit to the data, are added as a guide to the eye. We note that the standard deviation is roughly 15% very near the particle surface and decreases to 5% away from this surface.

fillers inside the notch increases as the size of the fillers is increased. For the system containing particles of size $\sigma_p = 1.8\sigma$, the volume fraction in the smaller notch is roughly 2.5 times the value for the uniform distribution. The majority of these particles are situated at the tip of the notch, similar to the scenario in Figure 3a, which is for the 1.7σ particles.

The main reason that the particles are localized at the walls (including the walls of the notch) is the polymer-induced depletion attraction between these fillers and the solid boundaries. Through mean-field calculations on particle-filled copolymer films, we recently showed that the confined chains gain conformational entropy by "pushing" the particles to the walls.[2,3] This depletion attraction is less pronounced for smaller particles because the chains can readily extend around them without significant stretching and loss of conformational entropy.[7,9−12]

To illustrate the above point through these MD studies, we place a single particle among 100 chains (each made up of 40 monomers) within a cubic lattice and measure the radius of gyration of the chains as a function of distance from the particle surface. Here, the size of the lattice is chosen such that the overall reduced density is 0.83, and periodic boundary conditions are applied in all directions. We carry out these simulations for particles with diameters of σ and 1.7σ. After the systems have reached equilibrium, we measure R_g^2 at different distances from the particle surface. In particular, we divide the range of radial values ($> r_c$, where $r_c = (\sigma_p + \sigma)/2$) into intervals of distance $\Delta r = \sigma/4$. We consider 120 000 configurations (over 12 million time steps) and monitor the distribution of the centers of masses of the chains around the particle. For polymer chains whose center of mass fall in a particular Δr, we increment a histogram table by the value of R_g^2 of the polymer. Dividing the total accumulation of R_g^2's by the total number of polymers whose center of mass fell within this interval allows us to calculate the average $\langle R_g^2 \rangle$ as a function of distance from the particle center. A plot of $\langle R_g^2 \rangle$ vs distance is shown in Figure 5. For both particle sizes, we see that near the particle surface, the chains are relatively stretched. As we go away from the particle surface, the chains relax and their $\langle R_g^2 \rangle$ value approaches the constant bulk limit. While the overall differences are not large for the particle sizes considered here, nonetheless, the value of $\langle R_g^2 \rangle$ is roughly 6% greater near the particle surface than in the bulk; for the smaller particle, the effect is on the order of 3%. From these data, we can deduce that if the particles are driven from the bulk of the film to the confining walls, the chain stretching would be diminished, and thus the polymers would gain conformational entropy. Since the extent of stretching is greater for the bigger particle, this effect is more pronounced for larger fillers. Our findings that the chains are stretched in the presence of the fillers is in qualitative agreement with recent computer simulations on the structure of bulk chains in the vicinity of solid nanoparticles.[30−32]

This argument can be extended to explain the significant particle accumulation at the tip of the notch (relative to the rest of the notch).[17−19] The confined chains could gain conformational entropy if the volume available to the polymers within the system were increased. The accessible volume can in fact be increased by driving the particles into the notch and particularly to the bottom of the notch. In effect, the depletion force is the highest when the particles effectively touch *both* walls of the notch. This *local* increase in the depletion attraction results in a higher concentration of nanoparticles at the notch tip.

B. Dynamics of the Particles. In addition to obtaining the equilibrium structure of the system, the MD simulations allow us to probe the dynamics of the system and measure the relative time scales that are required for the particles to migrate to and effectively fill the nanocrack. To carry out this study, we first model the pure polymer melt at a reduced density of 0.66 and equilibrate this system between the confining walls. We then introduce particles at randomly chosen positions within the melt such that the total reduced density becomes 0.83. Any overlap between particles and monomers is quickly removed using a short MD simulation with a softer cosine potential (see Models section above). Next, we substitute the Lennard-Jones potential for the cosine potential and begin to monitor the dynamics of the particles as they migrate toward the surfaces. The volume fraction of particles within the notch as a function of time is shown in the Figure 6 for particles with $\sigma_p = 1.7\sigma$; the data represents an average over seven independent runs.

We see that approximately 0.7×10^6 MD steps are needed before saturation is achieved; i.e., the number of particles inside the notch reaches an equilibrium

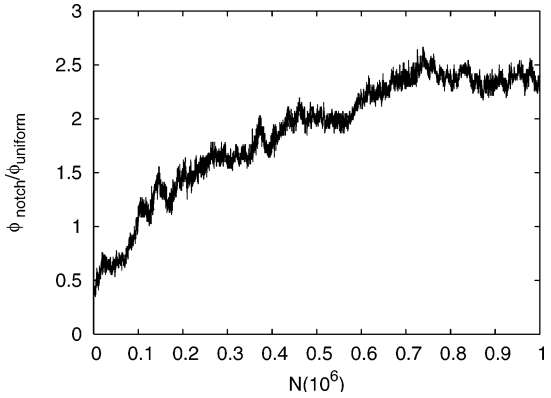

Figure 6. Average volume fraction of particles inside the notch as a function of MD time steps. Approximately $0.7 \times 10^6\tau$ are needed for the particles to migrate from the bulk into the notch and for the volume fraction of particles to reach the equilibrium value. Here, $\sigma_p = 1.7\sigma$.

value. The time needed for the center of mass of the polymer chains to move one R_g is approximately 0.2×10^6 MD steps. Thus, the saturation time for particles to migrate into the notch is of the same order as the time required for polymer chains to move on average by four R_g.

C. Mechanical Behavior of the System. The equilibrium polymer and particle distributions obtained from the MD simulations are directly fed into the LSM. Here, each σ unit in the MD simulation is represented by six lattice sites in the LSM. Our aim in these studies is to determine the effects of the nanocomposite coatings on the mechanical properties of the damaged substrate; therefore, we consider only the lower half of the MD simulation box, neglecting the top five σ layers near the top surface (see Figure 1b). We note that the LSM lattice extends 54 lattice sites (nine σ) below the notch.

The particles and substrate are considered to be 100 times stiffer than the polymer matrix. In addition, we assume that there is good adhesion between the particles and the monomers in the system, as would be the case if the particles and polymers are chemically compatible. We contrast the mechanical behavior of systems that are coated with a pure polymer layer (no particles) with the behavior of systems that are coated with the particle-filled polymer coating, where the particles are of size $\sigma_p = 1.7\sigma$. In this way, we can pinpoint the effects of the nanoparticles on the mechanical properties.

In the LSM, a deformation is applied in the lateral (x) direction. The normal stress field (σ_{xx}, where σ_{ij} is the stess tensor) for the case of a pure homopolymer coating is shown in Figure 7a, which shows the field through the system at $z = 0$. In addition, Figure 7c shows a contour plot of this system at $z = 0$ as well as

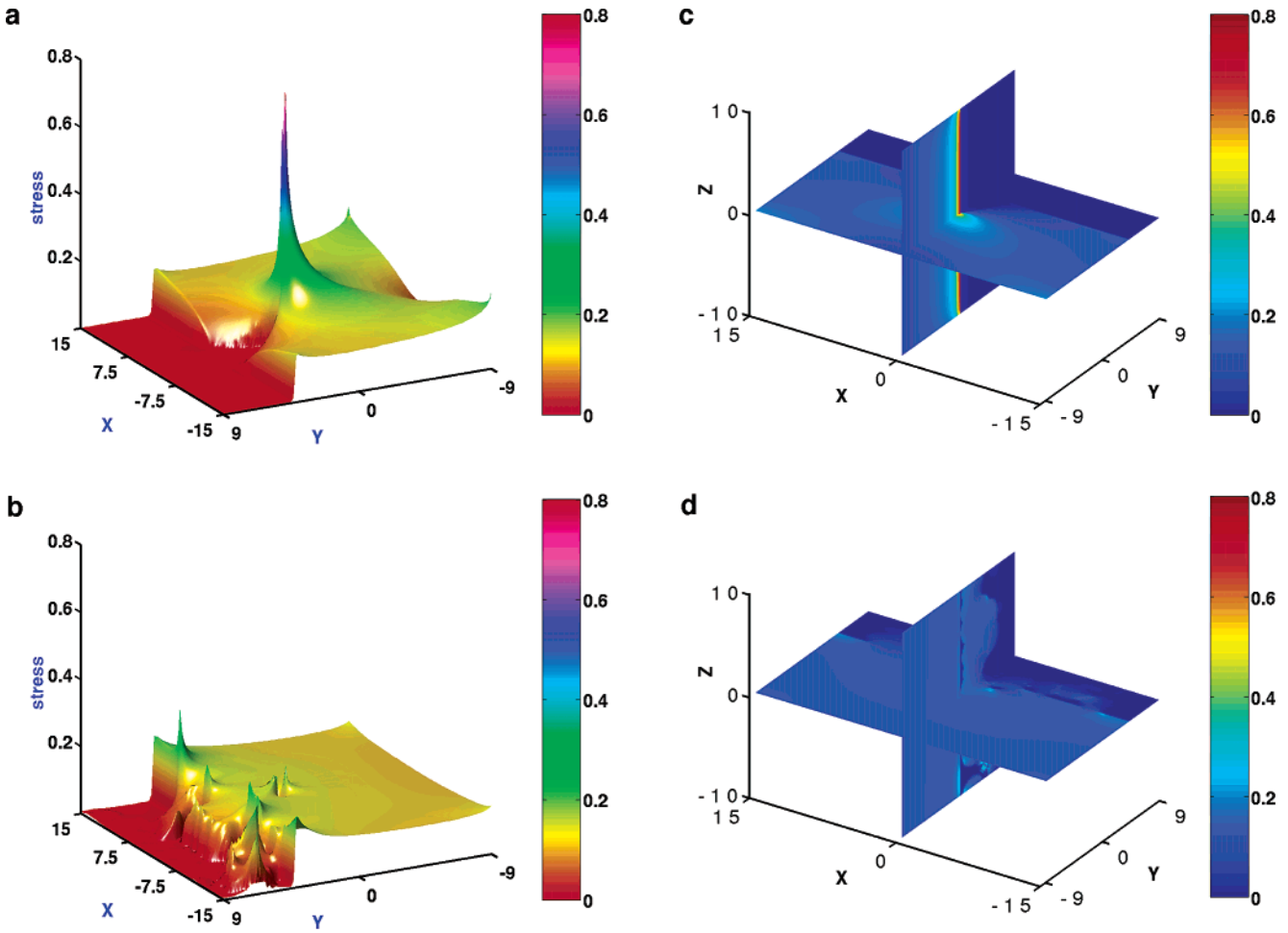

Figure 7. Two-dimensional profile (through the center of the simulation, at $z = 0$) depicting the normal stress field (σ_{xx}) in the following cases: (a) the absence of filler particles and (b) the presence of filler particles, where the particle size is $\sigma_p = 1.7\sigma$. Orthogonal contour slices depicting the normal stress field (σ_{xx}) in the following cases: (c) the absence of filler particles and (d) the presence of filler particles. The notch tip in these images is located at $x = 0$ and $y = 0$. The values for stress are in dimensionless units (since the Young's moduli are also expressed in dimensionless units).

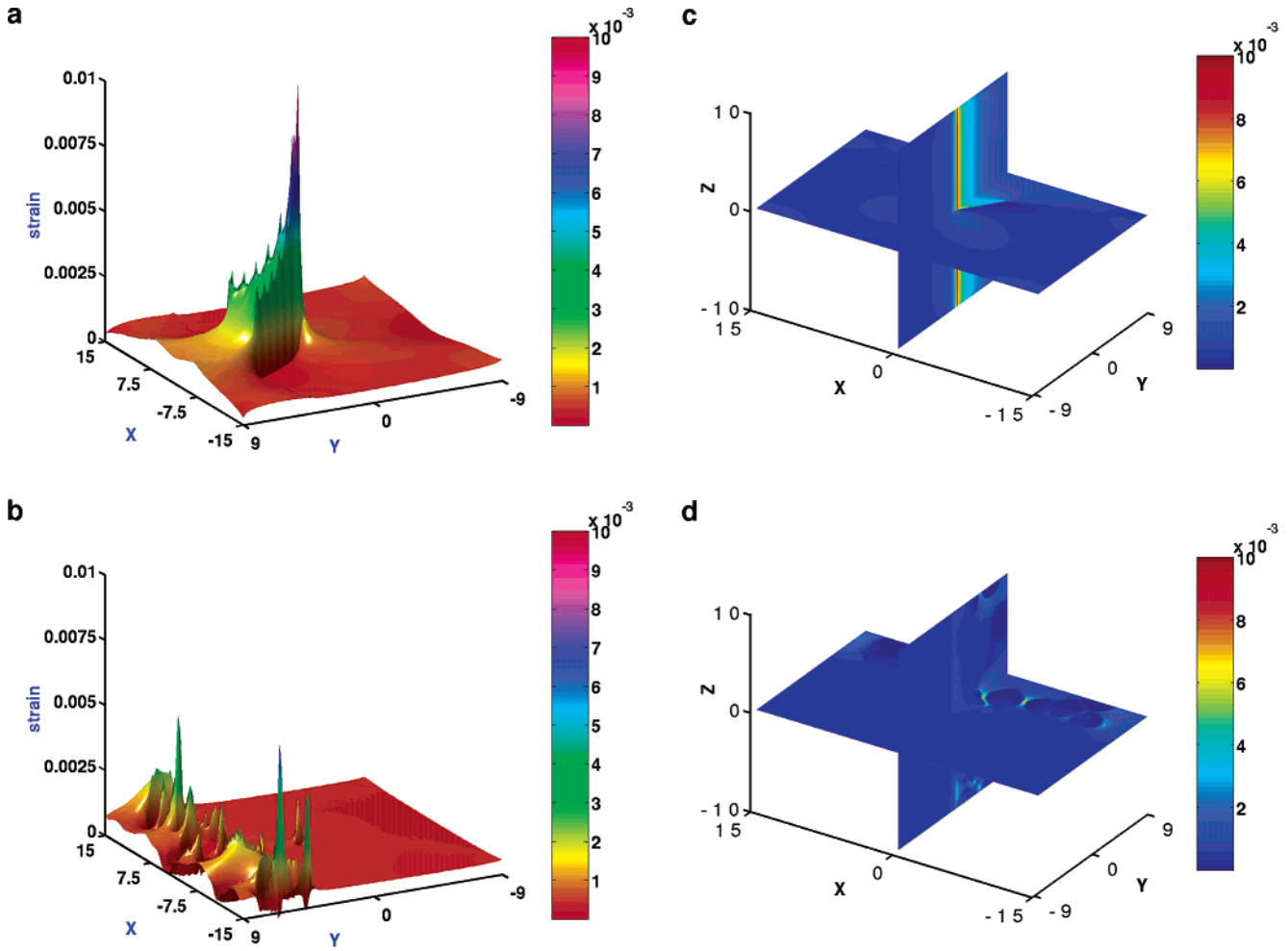

Figure 8. Two-dimensional profile (through the center of the simulation, at $z = 0$) depicting the normal strain field (u_{xx}) in the following cases: (a) the absence of filler particles and (b) the presence of filler particles (particle size $\sigma_p = 1.7\sigma$). Orthogonal contour slices depicting the normal strain field (u_{xx}) in the following cases: (c) the absence of filler particles and (d) the presence of filler particles. The notch tip in these images is located at at $x = 0$ and $y = 0$. (The values for strain are dimensionless.)

an orthogonal contour slice through the volume of the sample. It is seen that the stress is concentrated at the tip of the notch within the substrate. Such stress concentrations at the tips of surface defects can appear whenever the sample is subject to an external tensile load and are primarily responsible for the onset of crack propagation and the premature failure of the entire system.

The effect of filler nanoparticles in reducing the stress concentrations at the notch tip is shown in Figure 7b, which shows the field through the system at $z = 0$, and in Figure 7d, which shows a contour plot of this system at $z = 0$ as well as an orthogonal contour slice through the volume of the sample. The surface plots (Figures 7a,b and 8a,b) clearly depict the nature of the elastic fields, but we also plot the data as contour slices to illustrate the local variations in the fields due to variations in the particle distribution. The particles within the notch, and especially at the notch tip, act as a backbone of continuous reinforcing material that spans the notch and effectively *bridges* the surfaces of the notch. The stress is now transferred more through this reinforcing backbone and less through the substrate around the notch. It is clear from the contrast between parts a and b of Figure 7 (as well as between parts c and d) that stress concentrations at the notch tip are significantly reduced by the presence of the nanoparticles.

Figure 8a,c depicts the normal strain field (u_{xx}, where u_{ij} is the strain tensor) for the system coated with pure homopolymer, while Figure 8b,d shows the normal strain field for the system coated with the polymer nanocomposite. Without the introduction of the filler particles (Figure 8a,c), strain is concentrated in the soft polymer inside the notch. However, this strain is reduced in magnitude and becomes more evenly distributed throughout the sample in the presence of the filler particles (Figure 8b,d).

By calculating the crack tip opening displacement (CTOD), we obtain another measure of the deformation of the material close to the notch and thereby gain additional insight into the effects of the nanoparticles. The CTOD at a distance h from the tip of the notch is given as $(\delta(h) - \delta_0(h))/\delta_0(h)$, where $\delta(h)$ is the opening of the crack when subject to tensile deformation and $\delta_0(h)$ is the opening of the undeformed crack. The CTOD was measured at 120 different sections, each one $\sigma/6$ apart, along the invariant direction (z-direction) of the notch.

In Figure 9, the upper curve is for the case where the coating consists of pure polymer and the lower curve is for the system coated with the particle-filled polymer film. Again, the particles are of size $\sigma_p = 1.7\sigma$. The presence of nanoparticles within the coating, and their subsequent localization within the notch, is found to significantly reduce the CTOD (especially at a distance

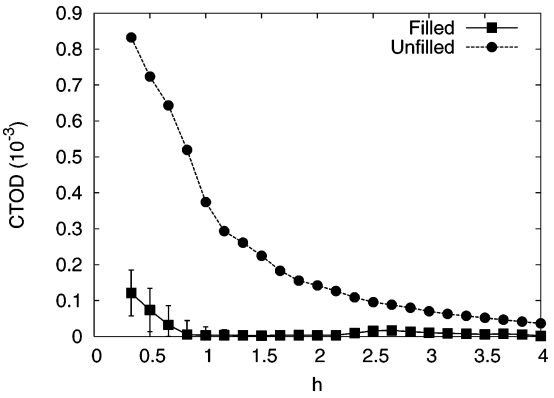

Figure 9. Effects of adding nanoparticles to the polymer coating on the crack tip opening displacement (CTOD). The line marked with solid squares is for the particle-filled case, while the line marked with solid circles is for the pure polymer case. In the former case, $\sigma_p = 1.7\sigma$.

of roughly a particle radius away from the notch, where the high concentration of particles reduces the CTOD to essentially zero).

IV. Conclusion

We integrated two computational models, the MD and LSM simulations, to determine the self-assembled structure of a nanocomposite coating and establish the mechanical properties of the coated substrate. This approach is particularly powerful since we can relate the distribution of the polymers and particles in the film to the mechanical behavior of that *specific* system. In this manner, we can ultimately establish fundamental structure−property relations for complex composite materials.

In these studies, the nanocomposite coating was applied to a damaged surface, which contained a nanoscale notch. We found that nanoparticles are driven to localize in the notch. The driving force for this localization is a polymer-induced depletion attraction; in other words, the confined polymers in the melt gain conformational entropy by "pushing" the fillers to the surfaces and into the notch. This behavior is analogous to that observed in solutions of binary colloidal particles that lie above a rough, corrugated surface.[17−19] In the latter situation, the smaller colloids in the solution can gain translational entropy by driving the larger spheres into the wells of the corrugated surface. By varying the size of the nanoparticles in our system, we found that the depletion attraction between the particles and the notch is more pronounced for the larger particles. Within the confined film, the polymers must stretch around the fillers, and the entropic penalty associated with the polymer stretching is greater for the larger particles. Thus, it is the larger particles that are more effectively expelled to the surface and the notch.

The density profiles from the MD show that the particles localize primarily at the bottom tip of the notch. A fraction is also localized in subsequent layers of this notch. As seen from the LSM calculations, these fillers significantly reduce the stress concentration at the notch tip relative to the case where the notched surface is just coated with a pure polymer layer. The calculations on the crack tip opening displacement indicate that the presence of the nanocomposite in the notch would inhibit the system from undergoing further damage (crack propagation from this notch) when an external load is applied to the system.

It is important to note that some fraction of the polymers are also localized in this damaged region. If the polymers and particles are chemically compatible, these chains provide cohesion between the fillers and the polymer coating. However, if the polymer and particles were incompatible, there would be little cohesion between these species, and the particles would decohere from the surrounding matrix, forming voids. Therefore, the chemical compatibility of the polymers in the gap also contributes to enhancing the mechanical properties of the system.

From the dynamic studies, we find that the larger particles can effectively migrate to the notch in relatively short time scales (comparable to the time needed for the chains to migrate over a distance of roughly four R_g), facilitating the experimental realization of this process. The application of such nanocomposite coatings could constitute an important processing step in the production of various components since this step has the potential to yield defect-free surfaces.

Acknowledgment. The authors gratefully acknowledge financial support from ARO, DOE, NSF, and ICI.

V. Appendix. Continuum Walls

Here, we discuss the modeling of the walls in the simulation. Initially, we can think of a wall made up of spherical particles of diameter σ located on a square lattice and spaced σ apart. We assume that the lattice extends to infinity in the $x-z$ plane. The potential energy at point y is given by summing over the contribution from the individual particle centers as follows

$$U(y) = 4\epsilon \sum_{m,n} \left[\left(\frac{\sigma}{r_{m,n}} \right)^{12} - \left(\frac{\sigma}{r_{m,n}} \right)^{6} \right] \tag{5.1}$$

where $r_{m,n} = (y^2 + m^2\sigma^2 + n^2\sigma^2)^{1/2}$ and the summation over m and n runs over $-\infty$ to $+\infty$. Next, we can imagine that the centers of the particles are only $\sigma/2$ apart. We obtain the energy at point y, but since the number of particles per unit area of the layer is 4 times greater than what we had before, we normalize the potential energy at point y by dividing by a factor of 4. We can imagine subdividing the separation between particles and then normalizing the energy again and again. This process will lead to the following normalized energy at point y

$$U(y) = 4\epsilon \int_{-\infty}^{+\infty} \int_{-\infty}^{+\infty} \left[\left(\frac{\sigma}{(x^2 + y^2 + z^2)^{1/2}} \right)^{12} - \left(\frac{\sigma}{(x^2 + y^2 + z^2)^{1/2}} \right)^{6} \right] \frac{dx}{\sigma} \frac{dz}{\sigma} \tag{5.2}$$

The integration over x and z can be easily performed. The integration over z yields

$$U(y) = \frac{3\pi}{64}\epsilon \int_{-\infty}^{+\infty} \left[21 \left(\frac{\sigma}{(x^2 + y^2)^{1/2}} \right)^{11} - 32 \left(\frac{\sigma}{(x^2 + y^2)^{1/2}} \right)^{5} \right] \frac{dx}{\sigma} \tag{5.3}$$

Then a final integration over x yields

$$U(y) = 8\pi\epsilon \left[\frac{1}{10} \left(\frac{\sigma}{y} \right)^{10} - \frac{1}{4} \left(\frac{\sigma}{y} \right)^{4} \right] \tag{5.4}$$

To keep the wall only repulsive in nature, one cuts off the potential at $y = y_c$ such that $\partial U/\partial y = 0$, which can be easily solved to obtain $y_c = \sigma$. Now eq 5.3 can be generalized to any arbitrary shape of the wall that is invariant along the z direction. Specifically, if we parametrize the surface with a curve $y = f(x)$, then the potential at point (x, y) will be given by

$$U(x,y) = \frac{3\pi}{64}\epsilon\int_{-\infty}^{+\infty}\sqrt{1+\left(\frac{\mathrm{d}f(x')}{\mathrm{d}x'}\right)^2}\left[21\left(\frac{\sigma}{g(x,y,x')}\right)^{11} - 32\left(\frac{\sigma}{g(x,y,x')}\right)^{5}\right]\frac{\mathrm{d}x'}{\sigma} \quad (5.5)$$

where $g(x, y, x') = [(x - x')^2 + (y - f(x')^2)]^{1/2}$. As before, to keep the wall only repulsive in nature, one can cut off the integration limits at those values of x' where $g(x, y, x') = (231/160)^{1/6}\sigma$, which is obtained by putting $\partial U/\partial s = 0$, where $s = x$ or y. From the above expression for $U(x, y)$, we can calculate the expressions for forces in x and y directions by taking gradients of $U(x, y)$ with respect to the position. The equations obtained for force components were integrated numerically to find the force components at the points of a finely laid grid close to the walls, and the values thus obtained were stored in a look-up table.

References and Notes

(1) Higgins, D. A.; VandenBout, D. A.; Kerimo, J.; Barbara, P. F. *J. Phys. Chem.* **1996**, *100*, 13794.
(2) Lee, J. Y.; Shou, Z.; Balazs, A. C. *Phys. Rev. Lett.* **2003**, *91*, 136103.
(3) Lee, J. Y.; Shou, Z.; Balazs, A. C. *Macromolecules* **2003**, *36*, 7730−7739.
(4) de Gennes, P. G. *Scaling Concepts in Polymer Physics*; Cornell University Press: Ithaca, NY, 1979.
(5) Bolhuis, P. G.; Louis, A. A.; Hansen, J. P. *Phys. Rev. Lett.* **2002**, *89*, 128302.
(6) Meijer, E. J.; Frenkel, D. *J. Chem. Phys.* **1994**, *100*, 6873.
(7) Huh, J.; Ginzburg, V. V.; Balazs, A. C. *Macromolecules* **2000**, *33*, 8085−8096.
(8) Liu, Z.; Pappacena, K.; Cerise, J.; Kim, J.; Durning, C. J.; O'Shaughnessy, B.; Levicky, R. *Nano Lett.* **2002**, *2*, 219−224.
(9) Lee, J. Y.; Thompson, R.; Jasnow, D.; Balazs, A. C. *Phys. Rev. Lett.* **2002**, *89*, 155503.
(10) Thompson, R.; Lee, J. Y.; Jasnow, D.; Balazs, A. C. *Phys. Rev. E* **2002**, *66*, 031801.
(11) Bockstaller, M. R.; Lapetnikov, Y.; Margel, S.; Thomas, E. L. *J. Am. Chem. Soc.* **2003**, *125*, 5276−5277.
(12) Thompson, R. B.; Ginzburg, V. V.; Matsen, M.; Balazs, A. C. *Science* **2001**, *292*, 2469.
(13) McCrum, N. G.; Buckley, C. P.; Bucknall, C. B. *Principles of Polymer Engineering*; Oxford University Press: Oxford, 1997.
(14) Kickelbick, G. *Prog. Polym. Sci.* **2003**, *28*, 83−114.
(15) For a review see: *Colloid Physics*, Proceedings of the Workshop on Colloid Physics, University of Konstanz, Germany, 1995; *Physica A* **1995** *18*.
(16) Tuinier, R.; Rieger, J.; de Kruif, C. G. *Adv. Colloid Interface Sci.* **2003**, *103*, 1−31.
(17) Lin K. H.; Crocker, J. C.; Prasad, V.; Schofield, A.; Weitz, D. A.; Lubensky, T. C.; Yodh, A. G. *Phys. Rev. Lett.* **2000**, *85*, 1770−1773.
(18) Dinsmore, A. D.; Yodh, A. G. *Langmuir* **1999**, *15*, 314−316.
(19) Dinsmore, A. D.; Yodh, A. G.; Pine, D. J. *Nature (London)* **1996**, *383*, 239−242.
(20) Mural, M.; Grest, G. S.; Kremer, K. *Macromolecules* **1999**, *32*, 595.
(21) Kremer, K.; Grest, G. S. *J. Chem. Phys.* **1990**, *92*, 5057−5086.
(22) Buxton, G. A.; Balazs, A. C. *Interface Sci.* **2003**, *11* 175−186.
(23) Buxton, G. A.; Balazs, A. C. *Phys. Rev. E* **2003**, *67*, 031802.
(24) Shou, Z.; Buxton, G.; Balazs, A. C. *Composite Interfaces* **2003**, *10*, 343−368.
(25) Buxton, G. A.; Balazs, A. C. *Phys. Rev. B* **2004**, *69*, 054101.
(26) Buxton, G. A.; Balazs, A. C. *Mol. Simul.* **2004**, *30*, 249−257.
(27) Buxton, G. A.; Care, C. M.; Cleaver, D. J. *Model. Simul. Mater. Sci. Eng.* **2001**, *9*, 485−497 and references therein.
(28) Buxton, G. A.; Balazs, A. C. *J. Chem. Phys.* **2002**, *117*, 7649−7658.
(29) Monette, L.; Anderson, M. P. *Model. Simul. Mater. Sci. Eng.* **1994**, *2*, 53−66.
(30) Doxastakis, M.; Chen, Y.-L.; Guzman, O.; de Pablo, J. J. *J. Chem. Phys.* **2004**, *120*, 9335−9342.
(31) Picu, R. C.; Ozmusul, M. S. *J. Chem. Phys.* **2003**, *118*, 11239−11248.
(32) Starr, F. W.; Schroder, T. B.; Glotzer, S. C. *Phys. Rev. E* **2001**, *64*, 021802; *Macromolecules* **2002**, *35*, 4481−4492.

MA048773L